Indian Journal of Chemistry
Vol. 60A, February 2021, pp. 220-227

Band gap engineering and photocatalytic activity of new trirutile structure $Zn_{1-x}Mg_xSb_2O_6$ ($0 \leq x \leq 1$) solid solution

Nagarajan Arunkumar*

PG & Research Department of Chemistry, Saraswathi Narayanan College, Madurai 625022, India

*E-mail : arun.snc.mdu@gmail.com

Received 10 August 2020; revised and accepted 03 December 2020

Solid solution of trirutile structure type antimonate $Zn_{1-x}Mg_xSb_2O_6$ ($0 \leq x \leq 1$) and its photocatalytic activity is reported here. Compound has been characterized by powder X-ray diffraction and the data confirms the formation of single phasic trirutile products throughout the solid solution. SEM reveals spherical shaped particles with an average particle size of 0.25 – 0.5 µm. EDAX analysis confirms the elemental composition. Raman spectral modes of $Zn_{1-x}Mg_xSb_2O_6$ characteristic of trirutile structure confirm Mg substitution into $ZnSb_2O_6$. UV – visible diffused reflectance spectra show optical absorption edge in the range of 370 – 318 nm. The band gap in the range of 3.35 – 4.05 eV has indicated the band gap engineering of $Zn_{1-x}Mg_xSb_2O_6$ ($0 \leq x \leq 1$) and is explained by electro negativity and band dispersion. All the compositions of $Zn_{1-x}Mg_xSb_2O_6$ have shown significant photocatalytic activity towards degradation of rhodamine B and it is maximum for $MgSb_2O_6$ whose remarkable photocatalytic activity is described here.

Keywords: Solid solution, Band gap engineering, Optical properties, Raman spectroscopy, Catalytic properties

Inorganic metal oxide semiconductor based photocatalysts have been studied for environmental remediation and hence, are widely employed for abatement of a variety of organic pollutants, waste water treatment and also water splitting[1,2]. Semiconductor oxide materials act as photocatalysts towards light-induced photochemical reactions due to its electronic structure characterized by a filled valence band (VB) and an empty conduction band (CB) separated by an appropriate band gap[3]. Such metal oxide-based semiconductor materials are investigated as potential materials not only for photocatalyic applications but also for many other applications such as optical devices, solar cells.[3-9] Band gap engineering by chemical substitution is a suitable method to tune the semiconductors for selected applications including photocatalysis. Antimonate based oxides of the formula MSb_2O_6 (M = Zn, Cd, Ca, Sr and Ba) having wide band gap are an significant class of photocatalyst.[2,10,11] $ZnSb_2O_6$, a well known photocatalyst, exhibiting interesting electrical and thermoelectric properties, is explored as sensor for NO_2, CO_2, O_2 and H_2S in concentration levels as low as 100 ppm[12-14]. $MgSb_2O_6$ is useful as electrode material for dye sensitized solar cells and gas sensor material.[15, 16]

MSb_2O_6 crystallises in two types of structures, trirutile and $PbSb_2O_6$ structure. Ionic radii of divalent A-site cation less than 0.8 Å belongs to trirutile structure, for example, MSb_2O_6 (M= Zn, Mg, Co, Cu, Ni, Fe). Increasing the ionic radius of A-site cation favours $PbSb_2O_6$ structure (M = Cd, Ca, Sr, Ba, Pb)[16, 17] Mineralogically, MSb_2O_6 (M = Zn, Mg) is known as ordenezite, bystromite and crystallizes in trirutile-type structure, which has the space group $P4_1/mnm$. Its structure is built up from two edge-sharing SbO_6 octahedra along c axis, sharing their corners with two other SbO_6 octahedra. M atoms are octahedrally coordinated by six O atoms in each rutile unit. The topographies are (1) Dominant Sb 5s orbitals at the bottom of conduction band and (2) Edge-shared MO_6 octahedron (M metal) aligned regularly in the trirutile-type structure.[13,16-18] All these antimonates based photocatalyst contain distorted Sb–O polyhedral which is ascribed for their photocatalytic activity.[2]

Here we report new trirutile solid solutions $Zn_{1-x}Mg_xSb_2O_6$ for the first time along with its optical band gap engineering. It shows significant photocatalytic activity, for degradation of rhodamine B (RhB) and more importantly, $MgSb_2O_6$, though it is known for many years, its photocatalysis is reported for the first time here.

Materials and Methods

Materials

Starting materials for the synthesis of $Zn_{1-x}Mg_xSb_2O_6$ ($0 \leq x \leq 1$) were antimony trioxide 99.99% (Sigma Aldrich), zinc oxide 99.99% (Sigma Aldrich) and magnesium oxide 99.99% (Sigma Aldrich).

Preparation of $Zn_{1-x}Mg_xSb_2O_6$ solid solution

$Zn_{1-x}Mg_xSb_2O_6$ was prepared by standard solid-state method. Stoichiometric quantities of ZnO, Sb_2O_3 and MgO were mixed thoroughly. This mixture was heated at 600 °C for 12 h and finally at 900 °C for 6 h with intermediate grindings in a programmable thermolyne furnace (Model No: F46110CM-33) with a heating rate of 4 °C/min and then the furnace was cooled.

Characterization

The products were characterized by X-ray diffraction (XRD) using Bruker D8 Advance with Cu K_α radiation (λ = 1.5406Å). Surface morphology and microstructure were examined by a scanning electron microscope (FESEM Supra 55 - CARL ZEISS, Germany). Raman spectra were recorded on a laser Raman spectrometer (Horiba Scientific/Lab RAM HR). Band analysis was performed with a resolution in the order of 0.3 cm^{-1} to 1 cm^{-1}. Optical absorption properties of the products were measured by UV – visible diffused reflectance spectroscopy (DRS). Data were collected over the spectral range 200 –1200 nm using (Jasco UV-Vis-NIR V- 670, Japan). Baseline spectra were collected using $BaSO_4$ as a standard. Data were collected with a scan rate of 400 nm/min, at data interval of 1 nm and signal UV–visible bandwidth of 5 nm. Photodegradation reaction was carried out at room temperature under UV light irradiation from six medium pressure mercury lamps 8 W 254 nm UV lamps set in parallel to reaction tube. Heber multiamp photoreactor (model HML-MP-888) was used for photoreaction. For photocatalytic activity, 0.2 g of the photocatalyst was suspended in 100 ml of RhB (10 ppm) and this suspension was loaded in a photoreactor quartz tube. Before to irradiation the reaction mixture was stirred in the dark for 60 min to establish adsorption – desorption equilibrium between dye and photocatalysts. It was irradiated for different time periods using UV light. 2 ml of aliquots were draw from the reaction mixture at regular intervals (centrifuged to separate the photocatalyst) and the concentration of dye in the aliquots was continually monitored by measuring the absorbance at 554 nm, λ_{max} in a UV-visible-spectrophotometer (Hitachi - 2910). After completion of experiment, the photocatalyst was separated, dried at 100 °C and used for the next cycle. Total organic carbon (TOC) was estimated using TOC analyzer Elementar Vario TOC Select, Germany.

Results and Discussion

Structural Characterization

Powder XRD patterns Fig. 1(a) and (b) confirm single phasic products, ordered trirutile structure with characteristic reflections of (002), (101) and (112) throughout the solid solution $Zn_{1-x}Mg_xSb_2O_6$ ($0 \leq x \leq 1$). Above x = 0.5, the intensities of (222) and (312) reflections characteristics of $MgSb_2O_6$ are enhanced. All the compositions crystallize in tetragonal crystal system, space group $P4_2/mnm$ with a ~ 4.66(Å); c ~ 9.25(Å). The lattice parameters decrease with increasing Mg content following Vergard's law (Fig. 2). Zn^{2+} (0.60 Å) and Mg^{2+} (0.57 Å) ion are nearer ionic radii in size hence P-XRD pattern does not identified any significant shift due to near size of the Zn^{2+} and Mg^{2+} ion.

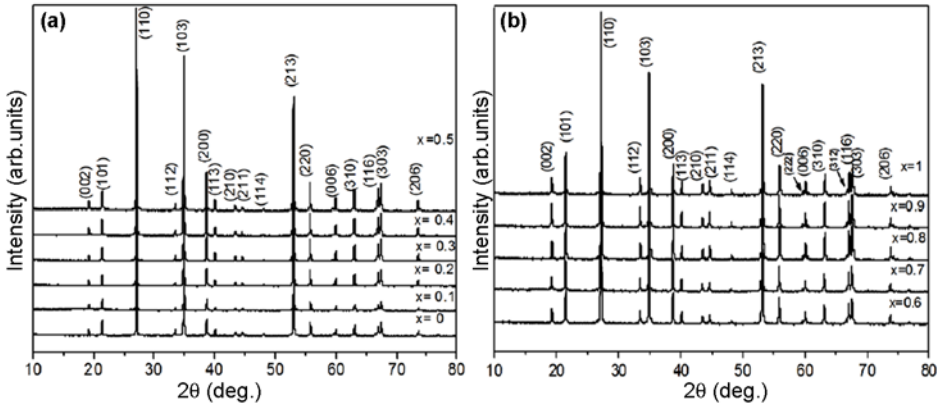

Fig. 1 — XRD patterns of $Zn_{1-x}Mg_xSb_2O_6$ (a) x = 0 to 0.5 and (b) x = 0.6 to 1

Surface morphology and microstructure

Surface morphology of $ZnSb_2O_6$ and $MgSb_2O_6$ as revealed by SEM analysis, shows spherical shaped morphology with average particles size in the range of 0.25 −0.5 µm (Fig. 3(a) and (c)). EDAX patterns shown in Fig. 3(b) and (d) confirm the cationic ratio to be equal to nominal chemical compositions and list out in Table 1.

Raman spectroscopy

Raman spectra for (x = 0; $ZnSb_2O_6$, x = 0.5; $Zn_{0.5}Mg_{0.5}Sb_2O_6$, x = 1; $MgSb_2O_6$ are shown in Fig. 4(a), (b) and (c). Raman spectra of $Zn_{1-x}Mg_xSb_2O_6$ ($0 \leq x \leq 1$) exhibit bands in the range 200 to 800 cm^{-1}, characteristic of trirutile structure indicates the single phasic nature of the products. According to the lattice dynamical calculations of the differences in all types of spectra are not due to vibrations of the MO_6 octahedra but mainly originate from vibrations of the Sb_2O_{10} units.[19-21] The bands occurring in the range of 500–800 cm^{-1} (A_{1g} and E_g) are related to vibrations involving Sb_2O_{10} units. The stretching vibration mode of the Sb–O bond appears between 600 and 800 cm^{-1}.[20-22] Trirutile structures belong to space group $P4_2/mnm$ and the corresponding Raman bands are observed in the range 200 to 800 cm^{-1}. Raman bands in the range 800 - 600 cm^{-1} correspond to simple bridging bond vibrations Sb − O_b − Sb, 600 - 500 cm^{-1} bands correspond to Sb − O_{cyc} vibrations and Sb – Ob − Sb vibrations coupled with M^{2+} − O vibration, bands in at range 500 - 200 cm^{-1} are due to M^{2+}–O vibrations.[23, 24] The systematic shift in Raman bands (Table. 2) also confirms Mg substitution in $ZnSb_2O_6$.

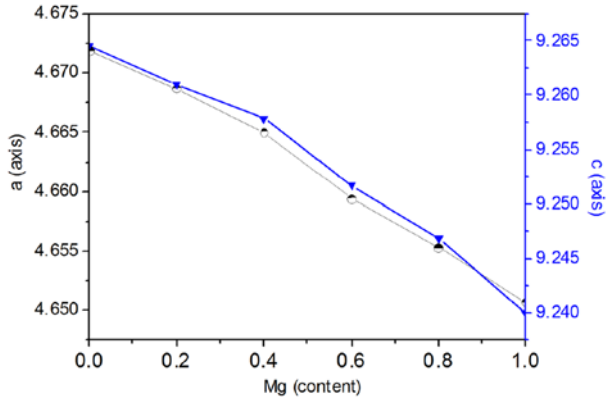

Fig. 2 — Lattice parameter variation with increasing Mg^{2+} content in solid solution $Zn_{1-x}Mg_xSb_2O_6$ ($0 \leq x \leq 1$)

Table 1 — EDAX data for the MSb_2O_6 (M = Zn, Mg)

Material	Atomic percentage (%) Zn/Mg Sb O
$ZnSb_2O_6$	11.84 20.98 67.18
$MgSb_2O_6$	11.24 21.92 66.84

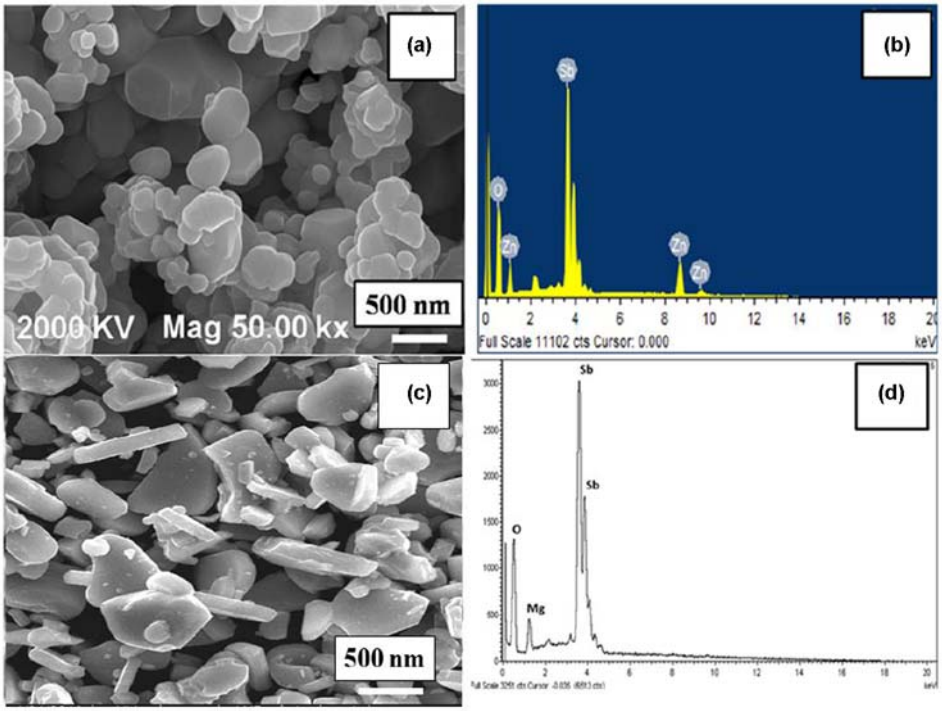

Fig. 3 — SEM and EDAX pattern of [(a) & (b)] $ZnSb_2O_6$ and [(c) & (d)] $MgSb_2O_6$

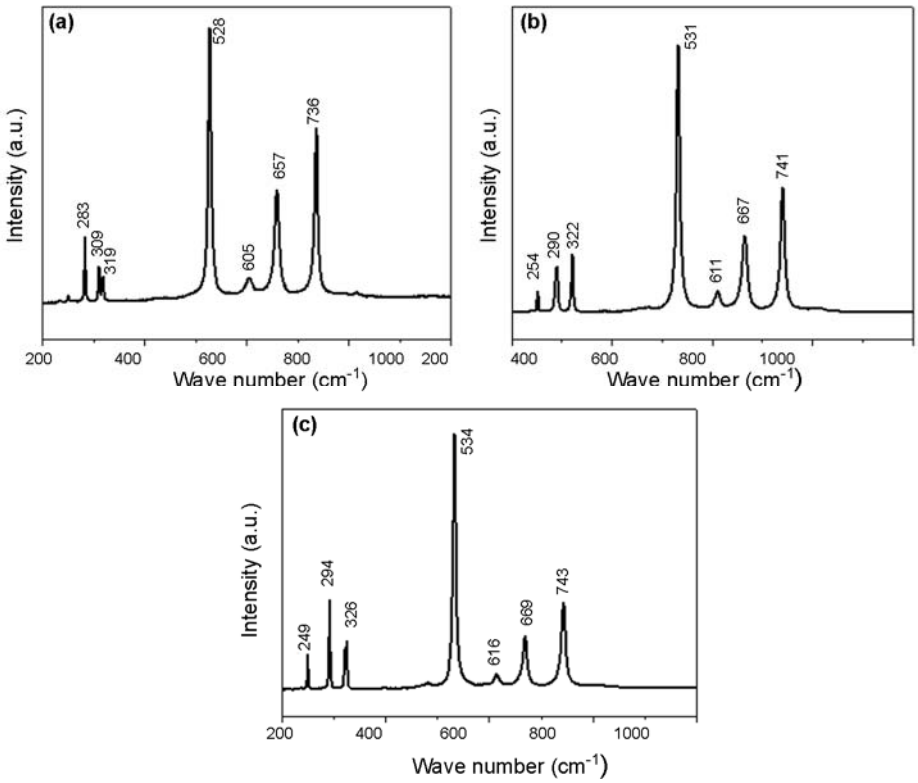

Fig. 4 — Raman spectra of $Zn_{1-x}Mg_xSb_2O_6$ (a) x=0, (b) x=0.5 and (c) x=1

Table 2 — Raman bands of $Zn_{1-x}Mg_xSb_2O_6$

Symmetry	Vibration Type	Raman displacement (cm^{-1})		
		x = 0	x =0.5	x = 1
E_g	Stretching (symmetric)	736	741	743
E_g	Stretching (symmetric)	657	667	669
E_g	Stretching (asymmetric)	605	611	616
E_g	Stretching and Coupling	528	531	534
A_{1g}	Crystalline Network	319	322	326
A_{1g}	Deformation	309	290	294
A_{1g}		283	254	249

Optical band gap

UV-visible DRS of $Zn_{1-x}Mg_xSb_2O_6$ in the range 200 − 1200 nm are shown in Fig. 5 (a). Reflectance increases with increasing Mg content. Reflectance is transformed to absorbance by using Kubelka - Munk conversion as given below.

$$(\alpha/S) = (1-R)^2/2R \quad \ldots (1)$$

Where α is absorption coefficient, S is the scattering coefficient and R is diffused reflectance at a particular energy.[13,25] The absorption spectra of $Zn_{1-x}Mg_xSb_2O_6$ shows one absorption edge and with increasing Mg content the absorption edge is shifted from 370– 318 nm (Fig 5b).Optical band gap is calculated using Tauc's relation Eqn (2): [7, 25, 26]

$$(\alpha h\upsilon)^{1/n} = A(h\upsilon - E_g) \quad \ldots (2)$$

Where, α denotes the absorption coefficient, hν is photon energy, A is proportionality constant, E_g is the band gap and exponent n depends on type of transition, n = 1/2 for direct transition. Optical band gap of $Zn_{1-x}Mg_xSb_2O_6$ increases with increasing Mg content and is in the range 3.35 − 4.05 eV (Fig 5c. Band gap increases upon replacing Zn^{2+} with Mg^{2+} indicating band gap engineering of $ZnSb_2O_6$ by chemical substitution. Band gap values of both end members are in good agreement with reported literature.[17] Increase in the band gap with increasing the Mg^{2+} content is caused by the conduction band (CB) dispersion and difference in electronegativity between Zn^{2+} and Mg^{2+}. In Zn^{2+} rich composition, there is more CB dispersion caused by Zn 3d and O 2p overlap. Due to less electropositive character of Zn^{2+} than Mg^{2+}, the valence band (VB) maximum is also pushed up resulting in smaller band gap. In Mg^{2+} rich composition the CB possesses significant antibonding character with O 2p destabilizing CB minimum, reducing CB dispersion and increasing band gap. This increase is also caused by more electropositive character of Mg^{2+} than Zn^{2+}

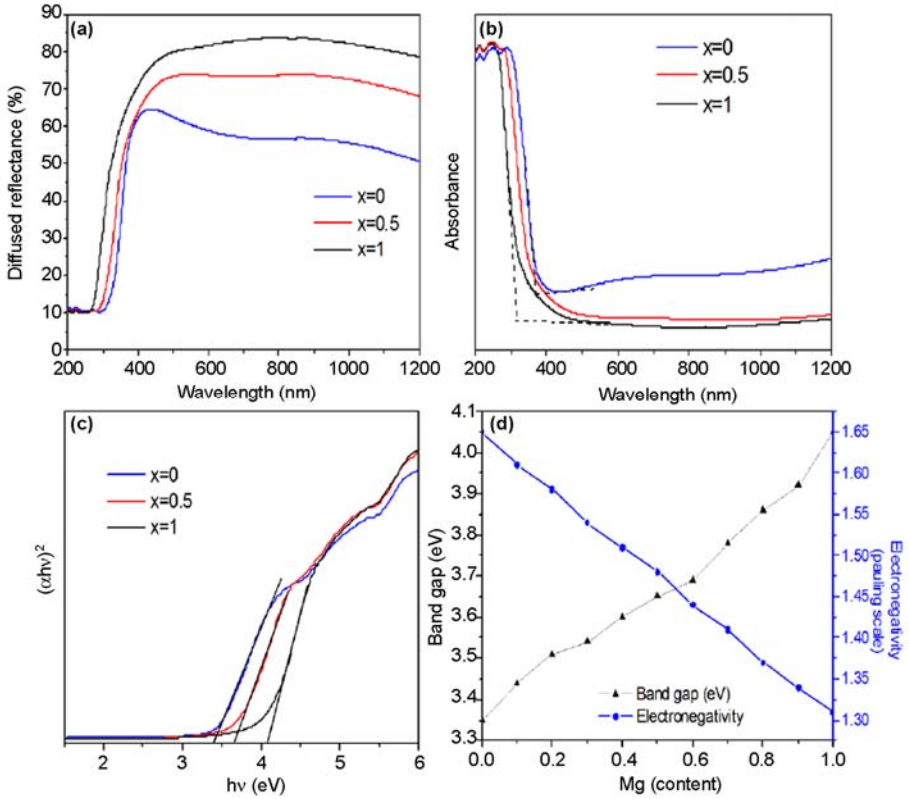

Fig. 5 — (a) Diffused reflectance spectra, (b) KM absorbance spectra, (c) Tauc's plot and (d) Band gaps vs. Mg-content plot $Zn_{1-x}Mg_xSb_2O_6$ where x=0, 0.5 and 1

and VB maximum is pushed down increasing the band gap.[17] Fig 5(d) shows band gap engineering of trirutile solid solution.

Photocatalytic activity

Photodegradation of organic dyes has been investigated in some detail for MSb_2O_6 (M = Zn, Cd, Ca, Sr, Ba, Pb & Co).[2,7,10,11,18,27] For example, nanocrystalline $ZnSb_2O_6$ and $CdSb_2O_6$ synthesized by hydrothermal method has been studied for degradation of RhB and methylene blue (MB), respectively.[2,10] MSb_2O_6 with larger M^{2+}ion (M = Ca, Sr, Ba, Pb) is reported to have significant photocatalytic activity towards the above dyes. Among these $BaSb_2O_6$ shows highest activity.[7,11] There is no report on the photocatalytic activity of $MgSb_2O_6$ and $Zn_{1-x}Mg_xSb_2O_6$ solid solution.

In the present work, we have investigated the photocatalytic performance of the compositions x = 0, 0.5 and 1.0 of $Zn_{1-x}Mg_xSb_2O_6$. It was evaluated by degradation of typical zwitter ionic dye (RhB) an organic pollutant, under UV light irradiations (λ = 254 nm). Sequential changes in the concentration of RhB monitored by measuring the absorbance at the wavelength, 554 nm (λ_{max}), are shown in Fig. 6(a), (b) and (c). Photodegradation of RhB dye is clearly observed for all the compositions and the maximum absorbance at λ_{max} (554nm) decreases with irradiation time due to stepwise degradation of conjugated chromophore content in RhB during photocatalytic process.[28] The temporal changes of RhB concentration during photodegradation is recorded as C/C_O where C is concentration of RhB at particular irradiation time and C_O concentration at zero point time (Fig. 7a).As Mg content increases photocatalytic activity increases at all irradiation time. The efficiency of degradation is shown in Fig. 7(b) and Table 3. Those compositions with high Mg content show maximum activity. Degradation efficiency of RhB for $ZnSb_2O_6$ is comparable with literature.[7] Remarkable photocatalytic activity of $MgSb_2O_6$ is reported for the first time here and is a more efficient photocatalyst than $ZnSb_2O_6$.To compare the reaction kinetics of the photodegradation of *p*-BP quantitatively, Langmuir-Hinshelwood (L-H) kinetics model was applied as per pseudo first-order equation[28].

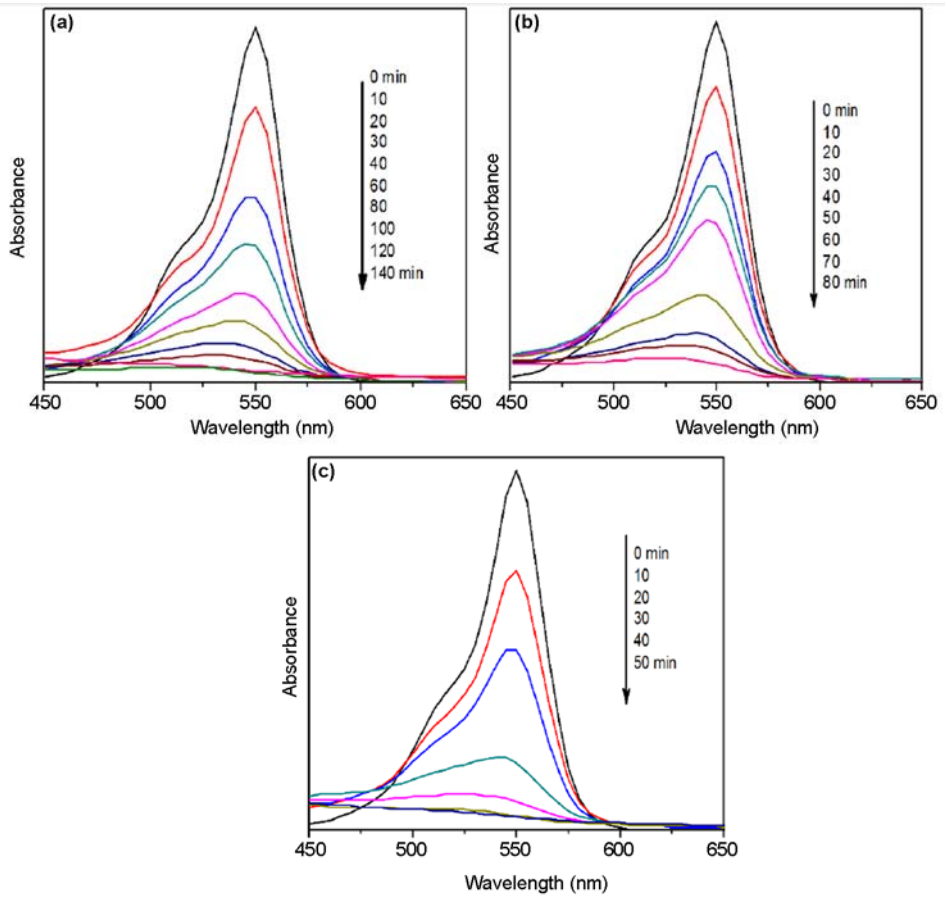

Fig. 6 — RhB photodegradation monitored by UV absorption spectra on the (a) $ZnSb_2O_6$, (b) $Zn_{1-x}Mg_xSb_2O_6$ (x =0.5) and (c) $MgSb_2O_6$

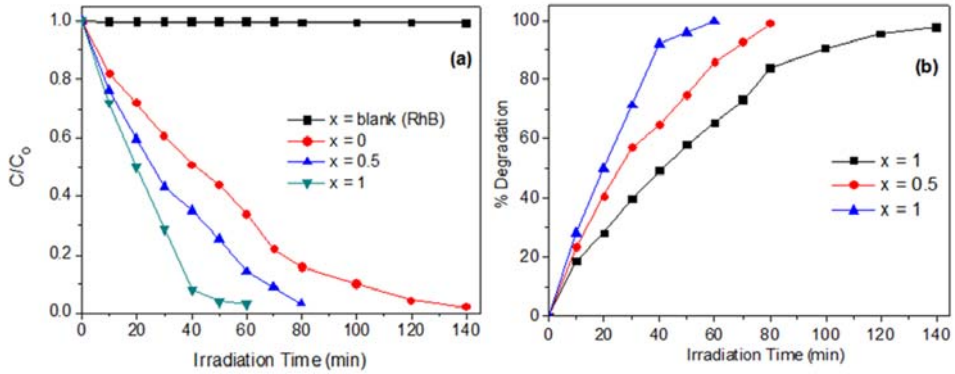

Fig. 7 — (a) Temporal changes of RhB concentration as observed by UV-visible absorption spectra at λ_{max} = 554 nm; (b) Percentage degradation of RhB with respect to irradiation time

Table 3 — Photocatalytic activity of $Zn_{1-x}Mg_xSb_2O_6$ solid solution under UV light irrdiation

Composition x	% Degradation	Irradiation time (min)
0	99	140
0.5	99	80
1	100	60

$$\ln (C/C_o) = - kt \quad \ldots (3)$$

The photocatalytic degradation kinetics of all the prepared products followed the expected first order which showed a linear correlation ($R^2 > 0.97$) between ln (C/C_o) and irradiation time.

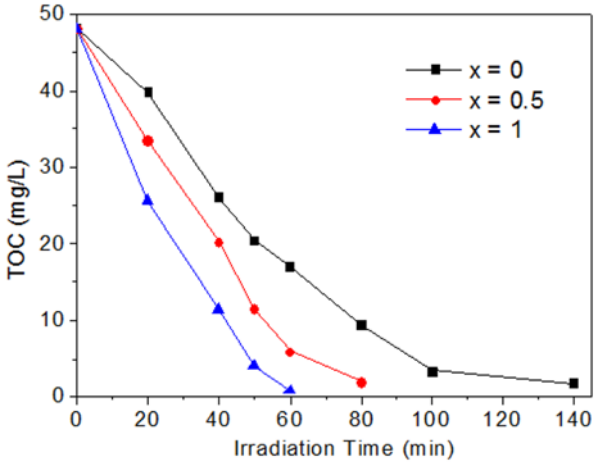

Fig. 8 — Disappearance of total organic carbon (TOC) during the UV light photocatalytic degradation of RhB with x = 0, x = 0.5 and x = 1

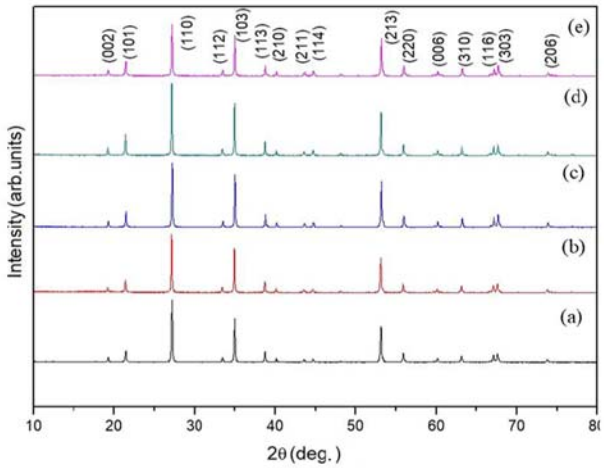

Fig. 10 — Powder XRD pattern of (a) as prepared $ZnSb_2O_6$ (e) as prepared $MgSb_2O_6$, Reusable photocatalyst after three runs (b) x = 0, (c) x = 0.5 and (d) x = 1

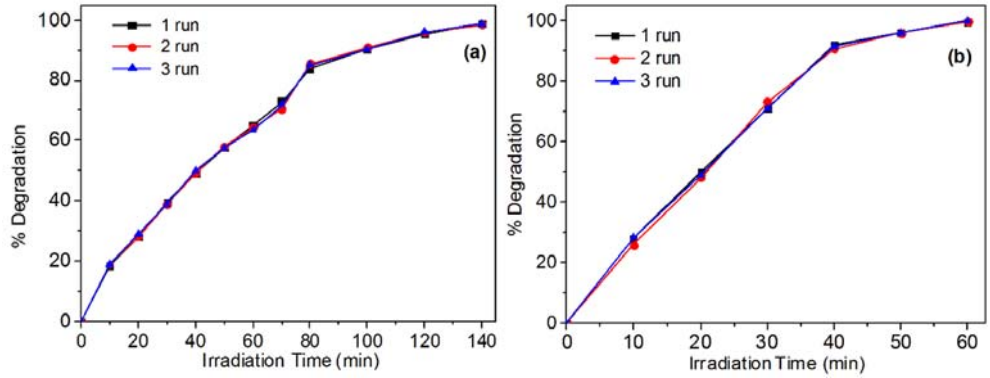

Fig. 9 — Recyclability plot for (a) $ZnSb_2O_6$ and (b) $MgSb_2O_6$ photocatalyst

Total organic carbon (TOC) measurements

TOC estimation for photocatalyst $Zn_{1-x}Mg_xSb_2O_6$ is plotted in Fig. 8. Decrease in TOC content with irradiation time reveals degradation (or) mineralization by the photocatalyst. RhB photodegradation occurs via two steps, first based on N-demethylation and then the breaking of conjugated structure due to degradation of conjugated chromophore content in RhB. So, RhB is converted to smaller organic species and finally is mineralized to inorganic products such as CO_2 and H_2O.[29,30]

Stability of photocatalyst

The stability and recyclability of $ZnSb_2O_6$ and $MgSb_2O_6$ photocatalysts were carried out for three runs under the same experimental conditions as shown in Fig. 9(a) and (b). No noticeable variation was observed between the cycles, revealing that these photocatalysts can be recycled. Powder XRD pattern of reusable photocatalyst is shown in Fig. 10 (a) – (e). There was no structural change in the compound was noticed after the three run.

Conclusions

Our study illustrates the band gap engineering of trirutile antimonite $Zn_{1-x}Mg_xSb_2O_6$ solid solution for photocatalytic application. XRD and Raman spectra confirm single phase formation with trirutile structure. Band gap value is tuneable in the range 3.35 to 4.05 eV and is explained in terms of electronegativity and band dispersion. Solid solution shows significant photocatalytic activity and $MgSb_2O_6$ shows highest activity. This solid solution could be explored for other applications such as water splitting, waste water treatment.

References

1 Li Q, Meng H, Zhou P, Zheng Y, Wang J, Yu J & Gong J R, *ACS Catal*, 3 (2013) 882.

2 Liu W, Lin P, Jin H, Xue H, Zhang Y & Li Z, *J Mol Catal A: Chem,* 349 (2011) 80.

3 Kumar S G & Devi L G, *J Phys Chem A,* 115 (2011) 13211.

4 Xia Y, Huang F, Wang W, Wang A & Sh J, *J Alloys Compd*, 476 (2009) 534.

5 Jiang H, Wang Q, Zang S, Li J & Wang X, *J Alloys Compd,* 600 (2014) 34.

6 Wu S, Li G, Zhang Y & Zhang W, *Mater Res Bull,* 48 (2013) 1117.

7 Dutta D P, Ballal A, Singh A, Fulekar M H & Tyagi A K, *Dalton Trans,* 42 (2013) 16887.

8 Tang J, Zou Z & Ye J, *Chem Mater,* 16 (2004) 1644.

9 Chen C H, Chen K C & He J L, *Curr Appl Phys,* 10 (2010) 176.

10 Singh J, Bhardwaj N & Uma S, *Bull Mater Sci,* 36 (2013) 287.

11 Lin X, Wu J, Lu X, Shan Z, Wang W & Huang F, *Phys Chem Chem Phys,* 11 (2009) 10047.

12 Michel C R, Contreras N L L, Lopez-Alvarez M A & Martinez-Preciado A H, *Sens Actuators B: Chem,* 171-172 (2012) 686.

13 Kikuchi N, Hosono H & Kawazoe H, *J Am Ceram Soc,* 88 (2005) 2793.

14 Katsui A & Matsushita H, *Phys Status Solid A,* 203 (2006) 2832.

15 Jang J & Kim S J, *Jpn J Appl Phys,* 51 (2012) 10NE23-1.

16 Guillen-Bonilla H, Flores-Martinez M, Rodriguez-Betancourtt V-M, Guillen-Bonilla A, Reyes-Gomez J, Gildo-Ortiz L, Amador M De La L O & Santoyo-Salazar J, *Sensors,* 16 (2016) Article 177.

17 Mizoguchi H & Woodward P M, *Chem Mater,* 16 (2004) 5233.

18 Zhang K L, Lin X P, Huang F Q & Wang W D, *J Mol Catal A: Chem,* 258 (2006) 185.

19 Matsushima S,Tanizaki T, Nakamura H, Nonaka M & Arai M, *Chem lett,* 30 (2001) 1010.

20 GiereE O, Brahimi A, Deiseroth H J & Reinen D, *J Solid State Chem,* 131 (1997) 263.

21 HussonE, Repelin Y & Brusset H, *Spectrochim Acta A,* 35 (1979)1177.

22 Atri S, Uma S & Nagarajan R, *Mater Sci Semicond Process,* 119 (2020) 105226.

23 Haeuseler H, *Spectrochim Acta A,* 37 (1981) 487.

24 Bahfenne S & FrostR L, *Appl Spectrosc Rev,* 45 (2010) 101.

25 Sheets W C & Stampler E S, *Inorg Chem,* 47 (2008) 2696.

26 Sahoo P P & Maggard P A, *Inorg Chem,* 52 (2013) 4443.

27 Jamal A, Rahman M M, Khan S B, Faisal M, Akhtar K, Rub M A, Asiri A M & Youbi A O A, *Appl Surf Sci,* 261 (2012) 52.

28 Wu S, Li G, Zhang Y & Zhang W, *Mater Res Bull*, 48 (2013) 1117.

29 Chen C C, Zhao W & Zhao J C, *Chem Eur J,* 10 (2004) 1956.

30 Luan J, Ma K, Pan B, Li Y, Wu X & Zou Z, *J Mol Catal A: Chem,* 321 (2010) 1.